Geophysical Research Letters

Supporting Information for

Landslide Sensitivity and Response to Precipitation Changes in Wet and Dry Climates

Alexander L. Handwerger[1,2], Eric J. Fielding[1], Simran S. Sangha[1,3], and David P.S. Bekaert[1]

[1]Jet Propulsion Laboratory, California Institute of Technology, Pasadena, USA. [2]Joint Institute for Regional Earth System Science and Engineering, University of California, Los Angeles, Los Angeles, USA. [3]Earth, Planetary, and Space Sciences, University of California, Los Angeles, CA, USA.

Contents of this file

Additional Supporting Information (Files uploaded separately)

Text S1.

InSAR Processing and Analyses

JPL-Caltech ARIA automatically processed standardized interferograms with Sentinel-1 data between 2015 and 2021 for California. At the time this study was performed however the InSAR data were only processed up to early 2020 (Figures 2 and 3). ARIA produced interferograms with 3 nearest connected neighbors and year-long pairs. We used the ARIA-tools open-source package in Python (https://github.com/aria-tools) to download all of the interferograms covering California. We downloaded 13825 individual products which was equivalent to 1689 merged interferograms from ascending tracks 35, 64, and 137, and descending tracks 42, 71, 115, 144, 173 (the full list of the InSAR data used in this study are in Table S1). The ARIA-tools package combines adjacent products into merged interferograms. We found there were sometimes discontinuities in the merged interferograms that resulted during unwrapping between data frames. Interferograms containing discontinuities were manually identified and removed from our analyses for the landslide identification stage, but were included for the time series analyses of selected landslides because the individual landslides did not span these discontinuities.

In order to search for landslides, it is important to use local reference points to help further reduce long wavelength noise that can obscure the landslide signal. We selected 32 regional stable (i.e., no motion) reference points that were used to reset the InSAR data velocity values (Table S4) and facilitate landslide detection. Additionally, we removed noise by excluding pixels with coherence less than 0.4, and applied linear deramping, DEM error correction (Fattahi & Amelung, 2013), and tropospheric corrections (Jolivet et al., 2011) with the European Centre for Medium-Range Weather Forecasts (ECMWF) ERA-5 reanalysis data set.

Once we selected the 38 landslides for time series analyses, we subset both ascending and descending InSAR data for each landslide and reprocessed the time series using a new local stable reference point. We then selected either ascending or descending data, depending on which data showed the best quality landslide signal (Figure S2). Finally, we projected the line-of-sight time series onto the mean downslope direction of each landslide, assuming surface-parallel motion using:

$$D_{downslope} = \frac{D_{LOS}}{sin(\alpha - \beta)sin(\theta_{inc})sin(\theta_{slp}) + cos(\theta_{inc})sin(\theta_{slp})}$$

where α is the heading direction (in degrees, positive counterclockwise from north) of the radar platform in the horizontal plane, θ_{inc} is the incidence angle, β is the mean azimuth angle of the landslide (i.e., downslope direction heading) and θ_{slp} is the mean hillslope angle of the landslide (Liu et al., 2013). This downslope projection can provide more accurate estimates of the true landslide displacement magnitude.

Landslide Classification and Geometric Scaling

We classified landslide types as slumps, earthflows, and complexes. We used the classification from Handwerger et al. (2021) where "slumps are landslides with lower length/width aspect ratios and one primary kinematic zone. Earthflows are landslides with medium aspect ratios and one primary kinematic zone. And landslide complexes are landslides with higher aspect ratios that are composed of multiple kinematic zones or even multiple landslides that coalesce into a single landslide mass".

We estimated landslide thickness using geometric scaling relations developed for slow-moving landslides in California (Handwerger et al., 2021). Landslide scaling relations take the form of a power function defined as

$$V = c_V A^{\gamma} \text{ and } h = c_h A^{\zeta}$$

where γ and ζ are the scaling exponents and c_V and c_h are fit intercepts. See parameters in Table (S5)

Supplementary Figures

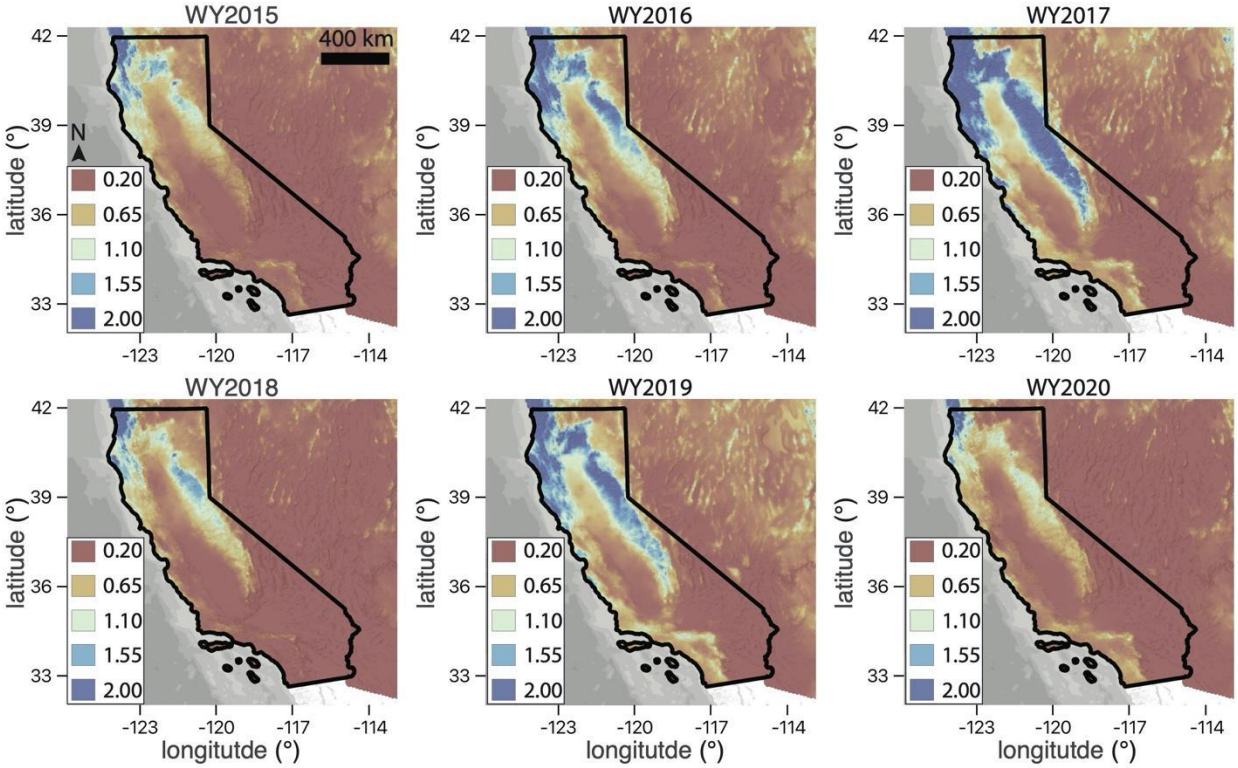

Figure S1. Water year precipitation maps. Colors show the total water year precipitation (m/yr). Data are from PRISM.

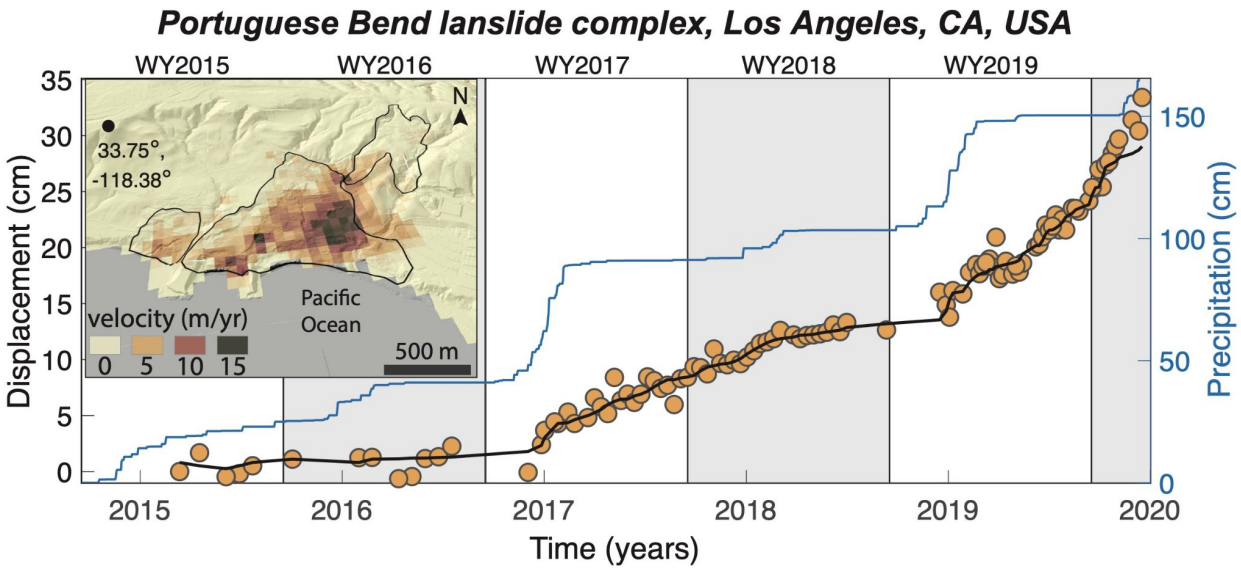

Figure S2. Displacement and precipitation time series for Portuguese Bend landslide. Orange circles show raw InSAR time series and black line shows smoothed time series. Displacement data are projected onto the downslope direction. Blue line shows cumulative precipitation time series. Inset shows oblique view of InSAR velocity map draped over a lidar hillshade. Black circle shows the location of the reference point for the time series and black polygons show active landslide boundaries.

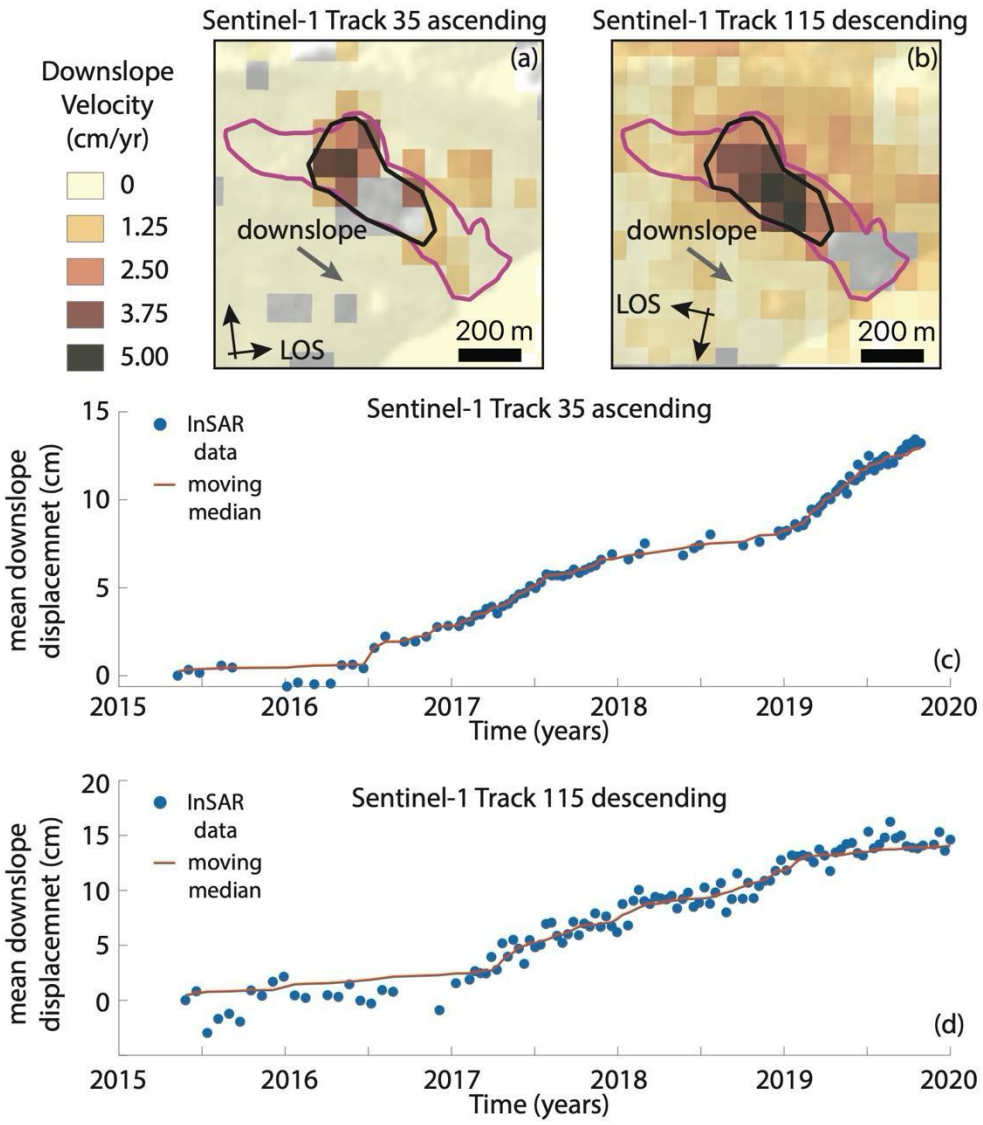

Figure S3. Example ascending and descending deformation maps and time series for a single landslide. (a-b) InSAR velocity maps draped over a hillshade of topography. Red colors show relatively high velocities. Magenta polygon shows the extent of the geomorphic landslide. Black polygon shows the fastest moving zone used to calculate the mean displacement plotted in (c-d). Arrows show downslope direction of landslide, satellite line-of-sight (LOS), and satellite flight heading. (c-d) Mean downslope displacement time series for ascending and descending InSAR data. Blue circles show the raw InSAR data and the orange line shows moving median smoothed time series.

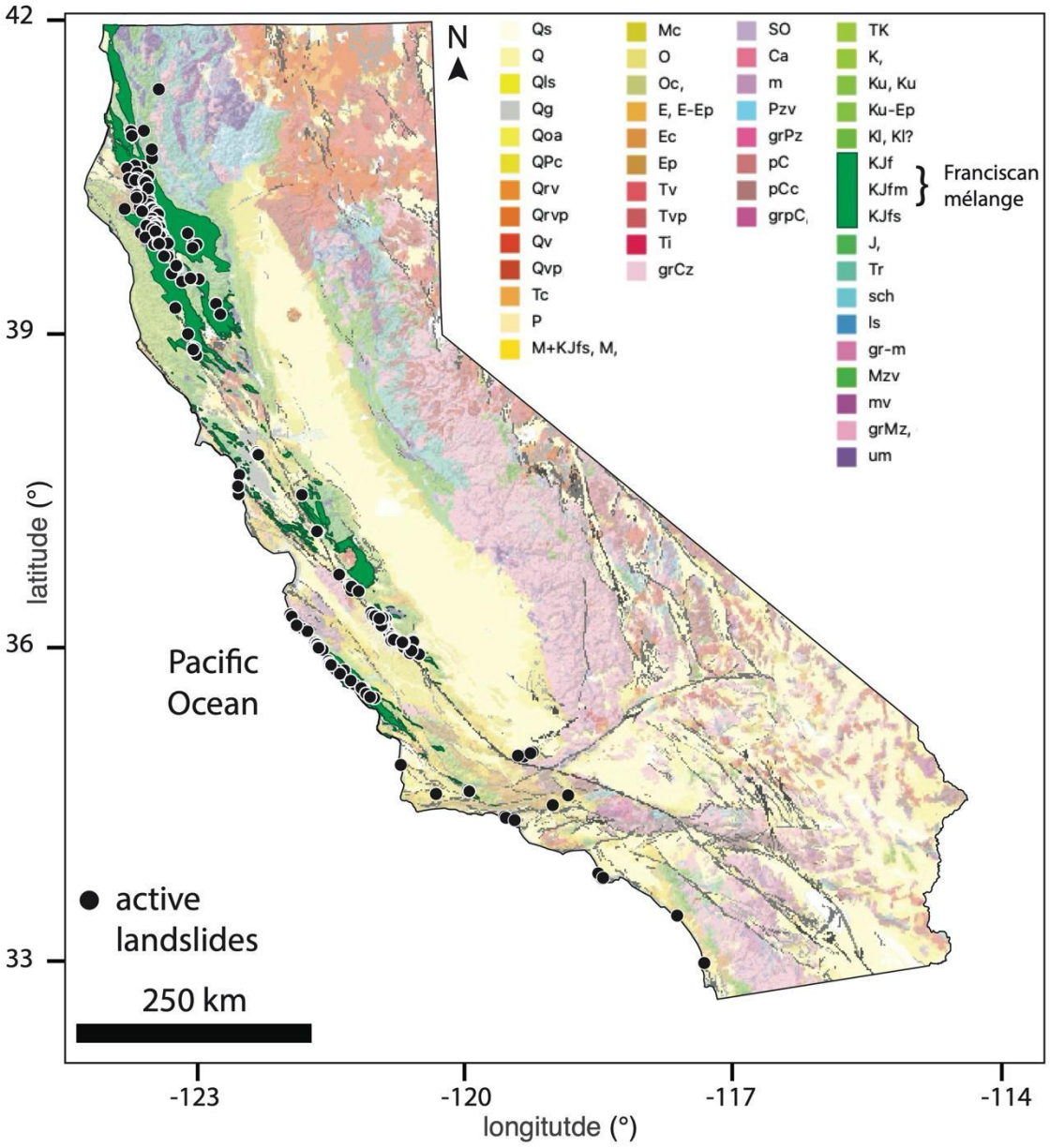

Figure S4. Geologic map of California. Black circles show location of active landslides identified with InSAR data. Data are provided by the California Geologic Survey. For detailed rock type descriptions see list at: https://maps.conservation.ca.gov/cgs/metadata/GDM_002_GMC_750k_v2_metadata.html.

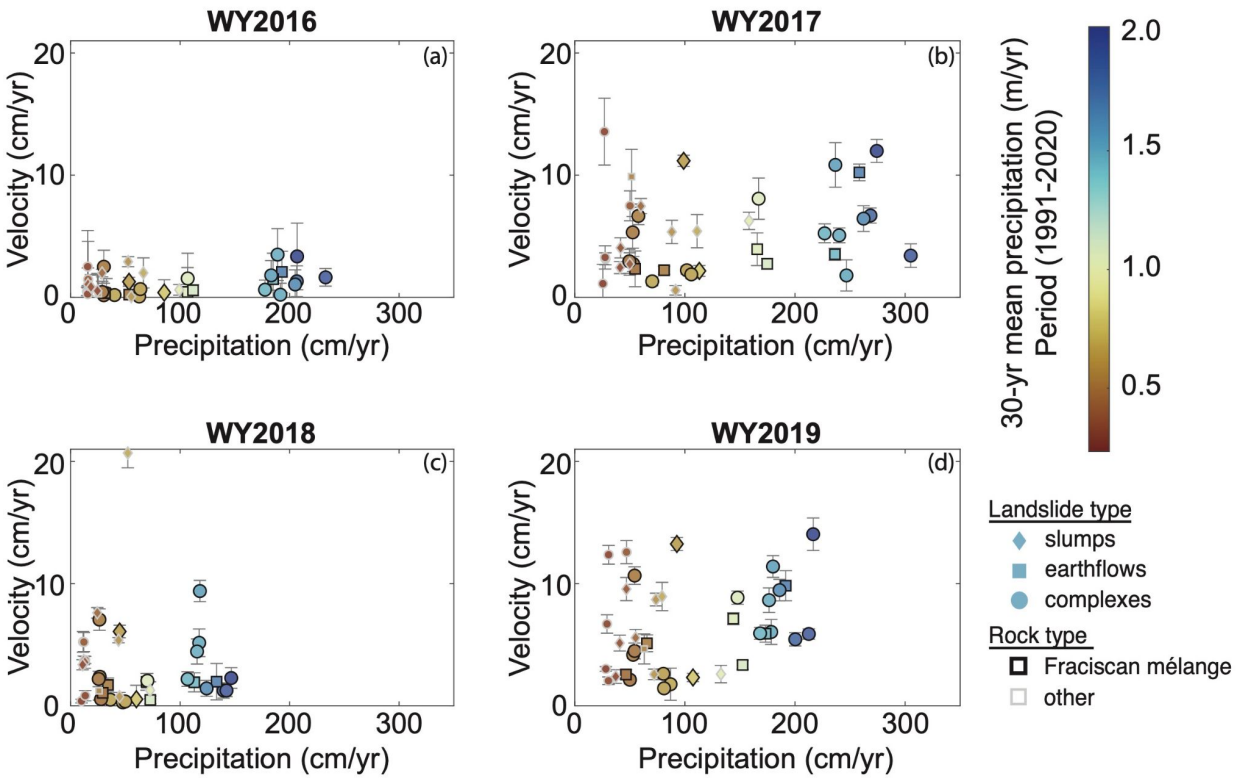

Figure S5. Landslide kinematics in response to changes in precipitation. (a-d) Water year (WY) velocity as a function of WY precipitation for selected landslides. Error bars show the uncertainty in the velocity estimates. Red to blue colors correspond to the 30 year normal precipitation (1991-2020) for each landslide. Symbols correspond to landslide type. Rock type is shown by black or gray symbol border color.

Supplementary Tables

Table S1. List of all InSAR pairs used in study. Columns correspond to the reference acquisition dates, secondary acquisition dates, perpendicular baseline, the timespan between images, and the total number of interferograms used in the time series inversion. The file contains eight spreadsheets that correspond to different satellite track numbers.

Table S2. Landslide inventory data table. Table includes information for landslide type, host rock type, mean slope angle, landslide area, landslide length, landslide width, centroid location of each landslide, and 30-year mean water year precipitation for each landslide (WY1990-WY2019).

Table S3. Landslide data table for the 38 selected landslides. Table includes information for landslide name, centroid location, landslide type, host rock type, landslide area, landslide length, landslide width, estimated landslide volume, estimated landslide thickness, mean slope angle, downslope aspect direction, InSAR data used for final time series analyses, stable reference point, and velocity and precipitation data.

reference point longitude (degrees)	reference point latitude (degrees)
-116.3914054	34.26675748
-116.5356684	33.8258261
-117.274774	32.844484
-117.646708	34.288767
-117.8200602	33.62590427
-118.3619388	33.76003981
-118.575646	34.042921
-118.67185	34.55515674
-119.632258	37.985456
-120.0213188	39.4384228
-120.021619	39.43817
-120.87114	36.272458
-121.0954394	36.74856042
-121.190797	36.622521
-121.445966	35.876472
-121.536581	36.026733
-121.585882	36.061785
-121.675278	37.344674
-121.7488595	37.46076441
-121.809952	36.26085
-121.8681335	37.15969
-121.886534	36.426898
-122.265977	37.31953
-122.290836	37.926315
-122.483311	37.699138
-123.050031	38.885312
-123.3293693	39.65829982
-123.393747	39.806784
-123.467188	40.106911
-123.800918	40.558561
-123.816244	40.987106

Table S4. Location of stable reference points used for landslide identification during the statewide mapping.

category	c_v, best fit intercept	γ, best fit power function exponent	c_s, best fit intercept	ζ, best fit power function exponent
inventory	0.2074 (0.0746, 0.5761)	1.306 (1.213, 1.399)	0.2074 (0.0746, 0.5761)	0.3058 (0.2129, 0.3987)
slumps	0.0301 (0.0020, 0.4569)	1.493 (1.224, 1.762)	0.0301 (0.0020, 0.4569)	0.4926 (0.2236, 0.7615)
earthflows	0.0207 (0.0013, 0.3389)	1.535 (1.273, 1.796)	0.0207 (0.0013, 0.3389)	0.5348 (0.2734, 0.7963)
complexes	0.9542 (0.1029, 1.2674)	1.172 (0.9858, 1.357)	0.9542 (0.1029, 1.2674)	0.1716 (-0.0142, 0.3573)

Table S5. Volume-area scaling fit values (with 95% confidence bounds). Table is modified from Handwerger et al., 2021.